

A characterization of the single-photon sensitivity of an electron multiplying charge-coupled device

Lijian Zhang¹, Leonardo Neves², Jeff S Lundeen¹ and Ian A Walmsley¹

¹ Clarendon Laboratory, Oxford University, Parks Road, Oxford, OX1 3PU, UK

² Center for Quantum Optics and Quantum Information, Departamento de Física, Universidad de Concepción, Casilla 160-C, Concepción, Chile

E-mail: l.zhang1@physics.ox.ac.uk

Received 20 November 2008, in final form 20 January 2009

Published 15 May 2009

Online at stacks.iop.org/JPhysB/42/114011

Abstract

We experimentally characterize the performance of the electron multiplying charge-coupled device (EMCCD) camera for the detection of single photons. The tests are done with the photon pairs generated from parametric downconversion (PDC). The gain, time response and noise performance of the EMCCD are characterized. In addition, we attempt to use the camera to measure the spatial correlations of PDC. The results reveal the capabilities and limits of the EMCCD as a single-photon-detector array for the applications of quantum optics, astronomy and microscopy.

1. Introduction

Photons have a rich structure associated with their continuous variable (CV) degrees of freedoms: spectral (time–frequency) and spatial (position–momentum). This structure can play an important role in quantum information processing based on photons. In particular, information can be encoded into the CV degree of freedom, enabling a photon to carry the d -dimensional generalization of the qubit, the ‘qudit’. This can dramatically increase the information content per transmitted photon. For the photons generated from a realistic parametric downconversion (PDC) source, over 8 bits ($d > 256$) and 10 bits ($d > 1024$) of information per photon can be achieved for the spatial [1] and spectral [2] degrees of freedom, respectively. These results enable higher data rates for various applications of quantum communication including quantum key distribution (QKD) [1–3]. Moreover, QKD with high-dimensional states has the advantage of increased sensitivity to eavesdropping [4]. Considering the CV degrees of freedom, PDC sources also produce high-dimensional entanglement between the photons in each generated pair. This entanglement can be used to violate Bell inequalities [5], and thus demonstrate that nature is either nonlocal or cannot be described by a local realistic theory or both. A unique aspect of this higher dimensional entanglement is that with it the critical detection efficiency loophole in the experimental violation

of these inequalities can be closed with current efficiency detectors [6, 7].

The manipulation and measurement of the spatial or spectral properties of photons requires different setups and detection devices that are commonly used in the laboratory. For the spectral degree of freedom, one requires nonstationary optical elements, such as shutters, phase modulators and especially detectors whose response time is in the femtosecond–picosecond range. These devices are difficult or impossible to build with current technology. On the other hand, elements with high spatial and angular resolutions are available, which makes the spatial properties easier to manipulate. There have been a number of experiments on the employment and detection of the spatial degree of freedom of single photons [3] or entangled photon pairs [8–10]. Most of these experiments employ one detector to scan the possible values of the momentum and position values, so in principle, the outcome of each measurement is binary: either the photon hits the detector or not. This effectively reduces the usable dimensions of information back down to that of a qubit. Thus, to access the full potential of the continuous spatial variable a large array of detectors should be used. Each detector in the array should have single-photon sensitivity, sufficiently high quantum efficiency and spatial resolution and low noise. This type of detector array has emerging applications in quantum imaging [11] and

spatially multiplexed photon-number-resolving detection [12]. Some candidate detector arrays include the multi-pixel photon counter (MPCC), the avalanche photodiode (APD) array [12] and the charge-coupled device (CCD). Among these options the CCD provides the largest potential number of pixels. There have been some experimental demonstrations [13, 14] using an intensified CCD (ICCD) to detect the spatial information of single photons. Recently another CCD for low light level detection has been developed. This CCD, the electron multiplying CCD (EMCCD), is expected to possess higher quantum efficiency and spatial resolution than the ICCD, though it also has its own defects.

Although the EMCCD has already been employed in astronomy [15], there is still no complete description of its performance in quantum optics applications, especially the experiments that are using non-classical light sources (e.g., single photons). In this work, we experimentally test crucial parameters of a typical EMCCD camera in this exacting region. The light source employed in our experiments is the spatially entangled photon pairs generated from PDC. We describe an experiment to use the camera to characterize the spatial correlations of this source. The measurement results reveal the feasibility and limits of such a camera when acting as a single-photon-detector array. The paper is organized as follows: in section 2, we provide a description of the spatial entanglement properties of PDC; in section 3, we introduce the principle of EMCCD operation. Tests of its major characteristics are described in section 4. In section 5, we discuss an experimental setup to employ the EMCCD to measure the spatial correlations of PDC and compare the experimental results with numerical simulations. We conclude in section 6.

2. The spatial properties of PDC

To characterize the performance of the EMCCD for the detection of the spatial entanglement of photon pairs, we first need to have a photon pair source with well-defined spatial properties. PDC satisfies this requirement. During the process of PDC, a pump photon with wave vector \mathbf{k}_p is incident on a nonlinear crystal and with a small probability it will split into two lower frequency photons, usually called signal and idler photons, with wave vectors \mathbf{k}_s and \mathbf{k}_i . The spectral and spatial properties of the photon pairs arise from the nonlinear crystal's optical dispersion. Since we aim to measure the spatial properties of PDC, interference filters are used to restrict the frequency of signal and idler photon to the degenerate situation $\omega_s = \omega_i = \omega_{p0}/2$. This decouples the spatial degree of freedom from the spectral degree of freedom of the photons. The resulting quantum state of this light, up to two photon component, is given by

$$|\Psi\rangle \approx |\text{vac}\rangle + \mu \iint d\mathbf{k}_s^\perp d\mathbf{k}_i^\perp f(\mathbf{k}_s^\perp; \mathbf{k}_i^\perp) |\mathbf{k}_s^\perp; \mathbf{k}_i^\perp\rangle, \quad (1)$$

where \mathbf{k}_s^\perp and \mathbf{k}_i^\perp are the transverse wave vectors of the downconverted modes. The first term of equation (1) is the vacuum state and the second term represents the two-photon state. In practice, the signal and idler modes are

usually at small angles to the longitudinal axis, which means $|\mathbf{k}^\perp| \ll |\mathbf{k}|$ for all the modes involved. We restrict our theoretical model to situations in which the transverse section of the nonlinear crystal is much bigger than the pump beam diameter and the crystal's length L along the pump is small compared to the depth of the focus of the pump. Under these conditions, the bi-photon amplitude is given by $f(\mathbf{k}_s^\perp; \mathbf{k}_i^\perp) = \alpha(\mathbf{k}_s^\perp + \mathbf{k}_i^\perp) \phi_L(\mathbf{k}_s^\perp - \mathbf{k}_i^\perp)$. The function $\alpha(\mathbf{k}_s^\perp + \mathbf{k}_i^\perp)$ is the angular spectrum of the pump transferred to the two-photon state. For a pump beam with Gaussian profile and beam waist w_0 , we have

$$\alpha(\mathbf{k}_s^\perp + \mathbf{k}_i^\perp) = \exp\left(-\frac{w_0^2}{4} |\mathbf{k}_s^\perp + \mathbf{k}_i^\perp|^2\right). \quad (2)$$

The function $\phi_L(\mathbf{k}_s^\perp - \mathbf{k}_i^\perp)$ is the longitudinal phase-matching function. For Type-I downconversion, where the idler and signal photons have the same polarization, it is given by

$$\phi_L(\mathbf{k}_s^\perp - \mathbf{k}_i^\perp) = \text{sinc}\left[\frac{L}{2} \left(\Delta k - \frac{|\mathbf{k}_s^\perp - \mathbf{k}_i^\perp|^2}{4K}\right)\right] \\ \text{with } \Delta k = 2K - k_p, \quad (3)$$

where $K = k_s = k_i$. When $\Delta k \neq 0$, equation (3) represents non-collinear PDC. The joint probability distribution in momentum is $P_{\text{PDC}}^m(\mathbf{k}_s^\perp; \mathbf{k}_i^\perp) \propto |f(\mathbf{k}_s^\perp; \mathbf{k}_i^\perp)|^2$. The marginal probability distribution of the transverse k -vector of each mode is defined by $P_{\text{PDC}}^m(\mathbf{k}_u^\perp) = \int \mathbf{k}_v^\perp P_{\text{PDC}}^m(\mathbf{k}_u^\perp; \mathbf{k}_v^\perp)$, and the conditional distribution is $P_{\text{PDC}}^m(\mathbf{k}_v^\perp | \mathbf{k}_u^\perp) = P_{\text{PDC}}^m(\mathbf{k}_u^\perp; \mathbf{k}_v^\perp) / P_{\text{PDC}}^m(\mathbf{k}_u^\perp)$, where u and v represent s and i respectively, or vice versa. In the thin crystal regime and using a Gaussian approximation of the sinc function, the marginal distribution and conditional distribution may be approximated by

$$P_{\text{PDC}}^m(\mathbf{k}_u^\perp) \propto \exp\left[-\frac{2\gamma L^2 \Delta k}{K} (k_u^\perp - \sqrt{K \Delta k})^2\right] \\ \text{with } \gamma = 0.193, \quad (4)$$

$$P_{\text{PDC}}^m(\mathbf{k}_v^\perp | \mathbf{k}_u^\perp) \propto \exp\left(-\frac{w_0^2}{2} |\mathbf{k}_u^\perp + \mathbf{k}_v^\perp|^2\right). \quad (5)$$

Equation (4) shows that the downconverted photons will emerge from the crystal distributed around cones centred on the z -axis. In the degenerate case, the circular section of these cones has the same radius for signal and idler photons, which creates, after accumulation of a lot of pairs, a figure like that sketched in the left inset of figure 5. This ring represents the transverse momentum distribution of the degenerate downconverted photons. Inside this region the transverse momentum of the signal and idler are anti-correlated. If this anti-correlation were perfect, the photons would be found in diametrically opposite points inside the ring as illustrated in figure 5. However due to the uncertainty in the transverse momentum conservation, introduced by the finite pump beam spatial distribution, each generated photon is only localized to within the correlation area defined by the width of $P_{\text{PDC}}(\mathbf{k}_v^\perp | \mathbf{k}_u^\perp)$.

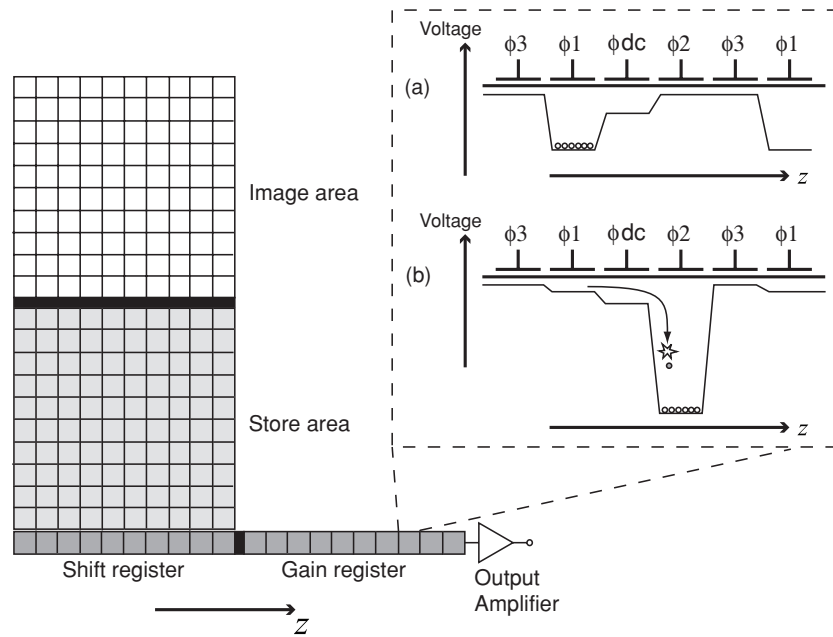


Figure 1. Schematic of EMCCD. Charges are driven across the shift and gain register by a sequence of voltage phases. The EMCCD achieves gain by applying a large voltage at phase ϕ_2 causing an avalanche multiplication of the number of electrons through impact ionization.

3. Principle of EMCCD operation

The structure of a standard frame transfer (FT) CCD consists of an image area, a store area, a shift register and an output amplifier. During the exposure time, a number of incoming photons hit the image area. A fraction of these, given by the quantum efficiency of the sensor chip, each generates a photo-electron. Once the exposure time has elapsed, the accumulated charges are rapidly transferred to the storage area, and then transferred vertically, line by line, to the horizontal shift register. From here the charges are transferred horizontally to the output amplifier. An EMCCD has the same structure, but with the shift register extended to include a section called the gain register (see figure 1). The gain register is similar to the shift register; it contains a line of discrete electrodes (see figure 1(a)) that are driven with a sequence of voltage to move the charges to the next element. The difference is that in a gain register element one of the three voltage phases (ϕ_2 in figure 1) is a high voltage pulse (typically 40–60 V) [16, 17]. Due to this high electric field the electrons transferred from ϕ_1 to ϕ_2 can experience impact ionization (or avalanche multiplication), which increases the number of electrons in the charge packet and provides gain. The gain per stage g is actually quite small, only around 1.01–1.015. But with a large number of stages N , a substantial total mean electron multiplication (EM) gain $G = g^N$ is achieved. For example, with $N = 520$ and $g = 1.015$, the total gain is over 2300. To ensure good dynamic range and gain stability and among other considerations, the actual gain is normally no bigger than 1000.

For the conventional CCD without a gain register, the detection limit is largely determined by the readout noise introduced by the output amplifier, which converts the accumulated charges into voltage. This noise is primarily

caused by resetting the amplifier for each pixel. It has a Gaussian distribution with the variance σ_{read} varies between several electrons to tens of electrons depending on the readout rate. The multiplication process in an EMCCD applies gain to the input signal prior to the output amplifier, reducing the effective readout noise to levels smaller than one electron rms. This makes single photo-electron detection possible. Ideally the same gain would be applied to every electron that passes through the gain register. Unfortunately due to the stochastic nature of the multiplication process there is no one-to-one mapping between the number of the input and output electrons. Rather, there is a large range in the number of output electrons that could be produced from each possible number of input electrons. In general, the probability distribution of the number of electrons x after the gain register, given n input electrons, can be approximated by [18]

$$p(x) = \frac{x^{n-1} \exp(-x/G)}{G^n (n-1)!}. \quad (6)$$

Figure 2(a) shows $p(x)$ for up to $n = 4$ with $G = 1000$. The dispersion in the number of output electrons increases the noise in camera signal and, through this, introduces uncertainty as to how many photo-electrons were at the input. In turn, this introduces uncertainty in the number of photons impinging on the camera. This camera noise is quantified by the excess noise factor (ENF) defined as

$$\text{ENF} = \frac{\sigma_{\text{out}}}{G\sigma_{\text{in}}}, \quad (7)$$

where σ_{in} and σ_{out} are the standard deviations of the input and output signals. When the input signal is single photocarrier ($\sigma_{\text{in}} = 0$), ENF can be defined as [19]

$$\text{ENF}_{\text{sp}} = \frac{\sqrt{\langle x^2 \rangle_{n=1}}}{G}, \quad (8)$$

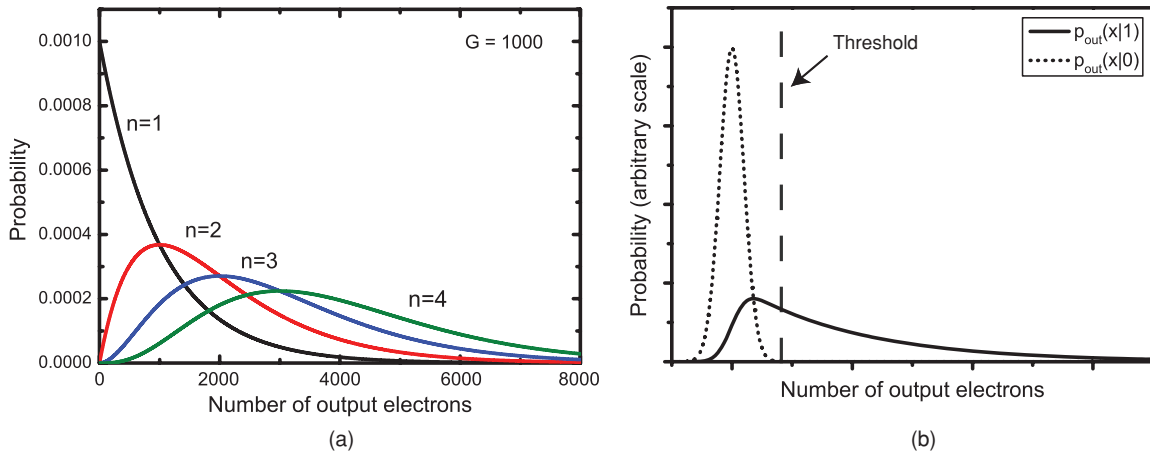


Figure 2. (a) The output probability distributions of the EM gain for 1–4 photo-electrons input. (b) The probability distributions after the output amplifier for no photo-electron and single photo-electron input. A threshold is used to distinguish between these two events.

where $\langle x^2 \rangle_{n=1}$ is the second moment of the output signal x when one electron is input³. It can be estimated from equation (6) that $ENF_{sp} = \sqrt{2}$. For coherent light input, where the photon number distribution is Poissonian, ENF tends to equal ENF_{sp} when the gain is high [16, 18, 19]. This noise performance is equivalent to that of a noiseless conventional CCD with half of the quantum efficiency. When the input signal level is low, e.g., no more than one photon/pixel, the EMCCD can be operated in a photon counting mode, i.e., any output signal above some threshold, which is much higher than the readout noise, is treated as arising from single-photon detection. Figure 2(b) shows the probability distributions of the number of electrons after the output amplifier of the EMCCD for two different input events. When there is no photo-electron input (the dotted line), the output is the readout noise, which has a Gaussian distribution $p_{out}(x|0)$ with variance σ_{read} . For single photo-electron input (the solid line), the output $p_{out}(x|1)$ is given by the Gaussian readout noise $p_{out}(x|0)$ convolved with the exponentially decaying amplified signal $p(1)$ for one photo-electron. To distinguish between zero and one input photo-electrons, the signals are thresholded at $6\sigma_{read}$: any signal above this level is treated as a photo-electron. Therefore, the probability that a photo-electron will be detected correctly is

$$P_t = \sum_{x=6\sigma_{read}}^{\infty} p_{out}(x|1) \approx \exp\left(-\frac{6\sigma_{read}}{G}\right). \quad (9)$$

P_t quantifies the capability of the camera to distinguish between the zero and one input photo-electrons, or the single-photon sensitivity of the camera. The effective quantum efficiency of EMCCD when it is operated in photon counting mode is

$$\eta_{eff} = \eta P_t, \quad (10)$$

where η is the quantum efficiency of photo-electron generation. If the gain is sufficiently high $G \gg \sigma_{read}$, we have $\eta_{eff} \approx \eta$, which shows that the photon counting mode removes

³ The definition of ENF_{sp} in [19] is the normalized second moment of gain, which is the square of equation (8).

the uncertainty introduced by the multiplication process and restores the lost quantum efficiency. However thresholding does have a drawback. As the input light intensity is increased, there is a growing chance that two photons will be absorbed by a single pixel. Thresholding will attribute the output signal to at most one photon, incorrectly. Basten *et al* have shown that the photon counting mode can be applied accurately up to 0.5 photon/pixel [18] for light with Poissonian input distribution. For the experiments described in this paper, we keep the input signal below this level.

4. Major characteristics of EMCCD

The EMCCD camera we employ in our experiments is the Andor iXon DV887DCS-BV X-1223, containing a CCD87 sensor from E2V Technologies. This CCD is commonly used in astronomy, but as far as we know, there is little work describing its performance in quantum optical experiments, especially for low light level (below one photon/pixel) detection. Consequently, we tested the main characteristics of the EMCCD relevant for single-photon detection. In this section, we will discuss the results of these tests.

4.1. General features

Table 1 shows some of the main parameters given by the manufacturer Andor Technology. The pixel size and number of pixels define the spatial resolution of the camera, which determine the configuration of PDC setup and the imaging system used in our experiment (see section 5 for more details). The readout mode, readout rate and clock speed define the temporal resolution of the camera, which will be discussed in section 4.2.

4.2. Time response features

The timing of detectors is an important issue for quantum communications, including quantum cryptography, where it sets the maximum transmitted key rate. It is also important for many quantum-optical applications involving coincident

Table 1. Values of the major parameters of Andor iXon DV887.

Description	Values
Pixel size (μm)	16×16
No. of pixels	512×512
Readout mode	normal imaging mode, frame transfer mode
Readout rate	1, 3, 5, 10 MHz
Vertical clock speed (μs) ^a	0.4, 0.6, 1, 1.8, 3.4, 6.6, 13
Pre-amplifier gain	$1\times$, $2.4\times$, $4.7\times$
Cooling method/temperature	-75°C with air cooling, -95°C with water cooling
Quantum efficiency (η)	75% at 810 nm, $\geq 50\%$ from 400 nm to 890 nm
Spurious charge (electrons/pixel/frame) ^b	≥ 0.005

^a This is actually the vertical shift time for one pixel.

^b See section 4.3 for more details.

detection of two photons, e.g., heralded single-photon sources, bipartite entanglement measurements, violation of a Bell inequality with entangled photon pairs, etc. Here, the detector time resolution sets the minimum time window with which the output signal can be gated. For avalanche photodiodes, the time resolution is limited by the avalanche jitter, which is around half a nanosecond, while for CCD camera, it is limited by either the shutter time or the minimum exposure time. If short enough, the exposure time itself could be used as a coincidence gating circuit between different pixels, ensuring that two detected photons were likely to have originated from the same emitted pair. Due to the special nature of its image intensifier, the intensified CCD camera can have shutter times as short as several hundreds of picoseconds, which is shorter than the 3 ns typically used in standard coincidence counting experiments (with APDs). In contrast the EMCCD camera uses an electronic shutter similar to normal CCD camera, which limits exposure times to no less than a few μs .

The Andor iXon DV887 camera can be operated in a non-frame-transfer mode as well as frame transfer mode, which have different minimum exposure times. In non-frame-transfer mode, the minimum exposure time is 20 μs and is not related to the other time settings of the camera. In the frame transfer mode, the exposure time has a minimum setting limited by the readout time, which is decided by the readout speed, the exposed area of the sensor and the number of pixels binned together. In our experiments, we usually operated in the frame transfer mode. To minimize the noise (see section 4.3), the readout speed is 1 MHz and the vertical shift speed is 0.4 μs . For this configuration the minimal exposure time is 0.02 s, which is much higher than the few nanoseconds typical in coincidence counting. Consequently, the photon pair-generation rate of the PDC light source should be reduced to minimize the chance that two unpaired photons are detected in the same pixel or diametrically opposite pixels with 0.02 s. The Andor camera is also equipped with a mechanical shutter, the operation time of which is tested to be 0.2 s by comparing the exposure level with and without this shutter. Our experiment results indicate that there are synchronization problems between the CCD and the mechanical shutter, and so the shutter is not used in the following experiments.

When the CCD camera is used as a detector array, another important issue is the time synchronization of different pixels of the CCD. CCDs are usually, but not always, equipped with a

global electronic shutter, enabling all the pixels to be exposed at the same time. To test whether the camera's exposure time control acts as a global shutter we use the attenuated pulses from a Continuum Powerlite Precision II 8000 laser as the input source. These pulses have a duration time of around 5 ns (FWHM) and a repetition rate of 10 Hz. The camera is configured to work in the frame transfer mode with an exposure time of 0.029s and a frame rate of 34.5 Hz. The laser beam is expanded to cover the whole area of the CCD sensor. If the pixels of the CCD are not synchronized to within 5 ns, during certain exposures some of the pixels will detect the input pulse while some will not, causing the resulting frames to have a nonuniform intensity distribution, i.e. bright areas interlaced with dark areas. We tested this over 10 000 frames and did not see this effect. So this is evidence that global electronic shuttering is used in this camera, and that the pixels are synchronized to within 5 ns.

4.3. Noise performance

Similarly to normal CCDs, the noise source of an EMCCD can be divided into off-chip noise (readout noise from the amplifiers, analog-to-digital quantizing noise, etc) and on-chip noise. As discussed in section 3, when the multiplication gain is sufficiently high, the contribution from off-chip noise is negligible. Excluding the multiplication gain noise as a separate type of noise, the on-chip noise consists of thermal dark current, spurious charge (also known as clock-induced charge, CIC), etc. These processes create electrons even when no light is impinging on the detector. These electrons are subsequently multiplied as described in section 3 and can result in false photon detections. Dark current occurs through the thermal generation of electron-hole pairs inside the semiconductors. Its contribution to the output signal can be greatly reduced by cooling the camera and keeping the exposure time as short as possible. CIC is generated when the camera is clocked during readout, and so it is mostly determined by the shape and frequency of the clock. In principle, CIC will increase slightly with the decrease of the operating temperature [20], but it has been shown that this increase is negligible for an EMCCD [21]. There are several points that a manufacturer needs to consider to minimize CIC, but for a user of the camera, there are very limited options and

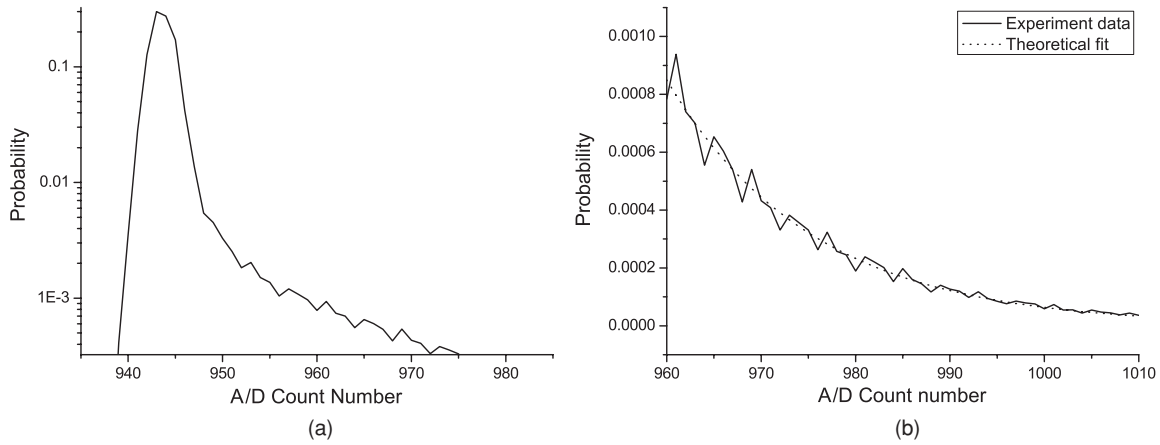


Figure 3. The noise performance of the iXon DV887 camera. (a) A histogram of the output digital signal per pixel for 2000 frames with a maximum multiplication gain and no input light. (b) A fit of the tail in (a) to an exponential decay in order to determine the noise contribution from clock-induced charge.

CIC sets the ultimate limit for the performance of EMCCD at low light levels.

To measure the noise performance of the iXon DV887 camera, we take a number of frames with the camera blocked, i.e., with no input signal. The histogram of the digitized output signal (arbitrary unit, DN) of the camera is shown in figure 3(a) with the multiplication gain set to be maximum, the vertical shift speed set to $3.4 \mu\text{s}$, readout speed set to 1 MHz and a temperature of $-75 \text{ }^\circ\text{C}$. As expected from section 3, the distribution of the noise is a weighted average of the two distributions (readout noise and single electron events) shown in figure 2(b). The Gaussian-like peak is solely due to the readout noise (in these events, no on-chip noise source created an electron), while the tail in the high DN region is the contribution due to multiplication of single electrons created through on-chip noise. In more careful examination, this tail is found to be largely independent of the exposure time indicating it is mostly from the CIC. By examining the width of the peak when the multiplication gain is turned off, the RMS of the readout noise (σ_{read}) is estimated to be less than 2 DNs. According to the manufacturer, for this readout speed there are 12 electrons per DN, so the readout noise is less than 20 electrons/pixel/frame. To estimate the CIC, we assume its distribution is similar to that of single photo-electrons given by equation (6):

$$p_{\text{cic}}(x) = \frac{n_{\text{cic}}}{G_{\text{cic}}} \exp(x/G_{\text{cic}}), \quad (11)$$

where G_{cic} is the mean gain and n_{cic} is the equivalent number of input electrons/pixel/frame to the CIC. Figure 3(b) shows the fit of equation (11) to the experiment data in the high DN region (more than $6\sigma_{\text{read}}$ away from the Gaussian peak). This gives the evaluation of $n_{\text{cic}} = 0.04$ electrons/pixel/frame and $G_{\text{cic}} = 180$. The minimum CIC we found for this camera is $n_{\text{cic}} = 0.005$ electrons/pixel/frame with vertical shift speed of $0.4 \mu\text{s}$ and readout speed of 1 MHz, which means there is on average one CIC electron/200 pixels/frame. Along with the input photon probability/pixel/frame, this sets the ultimate limit for the size of the useful area of EMCCD as a single-photon-detector array.

4.4. Multiplication gain

The multiplication gain G can be estimated in a similar way as G_{cic} : photon pairs generated from a PDC source are used as the input light to the EMCCD camera. The photon pair generation rate is first set to be high enough to allow the EMCCD camera to image the ring structure of PDC (figure 4(a)) during one exposure. An area A_{PDC} of 10×10 pixels is selected around an arbitrary point on the peak intensity circle in the ring. Then generation rate is lowered to ensure the maximum signal collected in A_{PDC} is much less than one photon/pixel/frame. A histogram of the EMCCD output signal from the pixels in A_{PDC} contains contributions from multiplied photo-electrons, multiplied CIC and the readout noise. We attempt to remove the latter two contributions by first recording histograms of the output signal within A_{PDC} , with and without light input. Each measurement has been done with 2000 exposures. The difference between the two histograms is due to single-photon events. We fit an exponential decay function to the tail of the difference between the two histograms (shown in figure 4(b)) and find that the detected number of photons is 0.152 photon/pixel/frame and the gain is $G = 247$. Comparison between G and G_{cic} shows that CIC noise experiences less gain than input signal. This agrees with our expectation that the CIC will be created in random point in the gain register and, thus pass through less multiplication steps. This is also confirmed by Tulloch [22].

From the measurement results in sections 4.3 and 4.4 and equation (9), if this camera is operated in photon counting mode, the effective efficiency will be reduced by a factor of $P_t = 0.67$. This rather large reduction is due to the low gain of this particular camera, which might be caused by the gain aging of EMCCD [23]. For another EMCCD camera we tested from Hamamatsu, we measured an EM gain of over 1000 and $P_t > 0.9$, evidence of the potentially superior quantum efficiency of the EMCCD.

4.5. Comparison between EMCCD and APD

To conclude this section, the detection efficiency of our EMCCD is compared with a standard silicon APD (Perkin

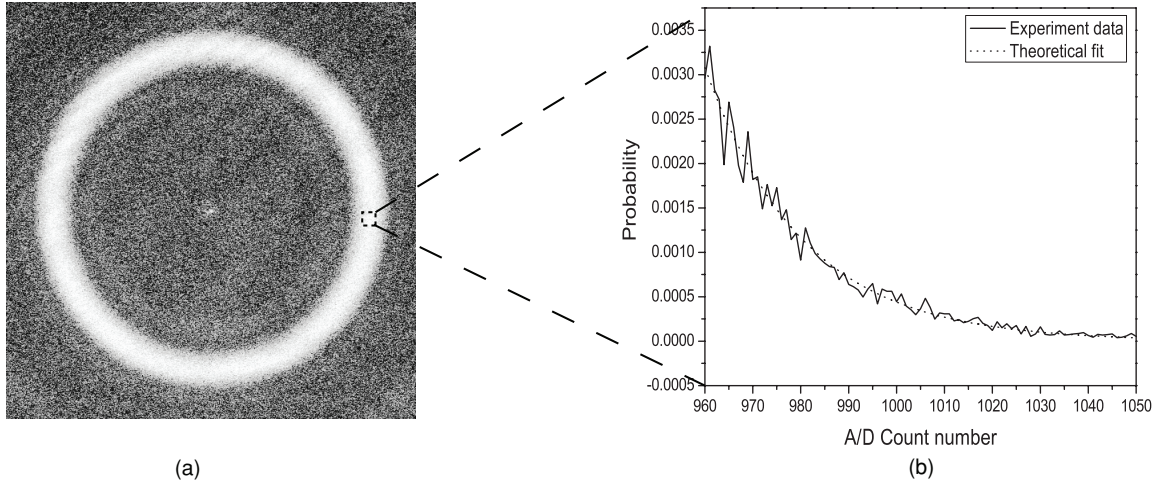


Figure 4. Measurement of the EM gain for a single-photon input. (a) The ring structure of PDC detected by the EMCCD. An area of 10×10 pixels around the peak intensity is selected to construct an output signal histogram. The histogram is used to determine the EM gain for a single input photo-electron. (b) The solid line is the histogram of the output distribution of single-photon events. This is fitted with an exponential decay function (the dotted line) to estimate the EM gain and the average number of detected photons/pixel.

Elmer, Model no. SPCM-AQR-13-FC 5387.Rev.F), which is the most widely used single-photon detector in quantum optics experiments. The attenuated Compass 405 (with a wavelength of 405 nm) laser diode pump is coupled into a single-mode fibre and used as the input light for both of the detectors. The intensity of the laser is adjusted to give around 18 000 clicks/s with the APD. The number of photons detected by the EMCCD is estimated with the method mentioned in section 4.4 to be 13 662 photons/s, which is close to that from the APD. Considering the additional loss introduced by the coupling into the camera, the intrinsic detection efficiencies η of the back illuminated EMCCD and APD are at the same level.

5. Characterizing spatial correlations of PDC with EMCCD

As mentioned in section 1, photon pairs generated from PDC exhibit a high degree of correlation in their spatial degree of freedom. But to access it requires a large array of detectors. From the various tests mentioned in section 4, EMCCD has single-photon sensitivity, good quantum efficiency and relatively low noise. However, it is still unclear whether the EMCCD can be used as a detector array in which each pixel in the camera acts as an independent detector, and thus has the ability to reveal the spatial correlations of the light. In this section, we discuss an experiment that employs the EMCCD to characterize the spatial correlations of PDC. The experiment results are compared with a numerical simulation of the EMCCD output signal, including all the factors discussed in section 4 and the difference reveals the capabilities and limits of the EMCCD camera.

5.1. The setup and the measurement method

Figure 5 sketches the setup to study the spatial properties of PDC with EMCCD. The output of a Coherent Compass 405 laser diode (with a wavelength of 405 nm) is spatially

filtered and then used to pump a 1 mm long BBO crystal to generate the Type-I PDC. An 810 ± 3 nm interference filter (IF) is used to select the degenerate photon pairs which propagate through an imaging system and are detected by the EMCCD camera. The focal length of the imaging lens is $f = 5$ cm. Both the distance between the crystal and the lens, and the distance between the lens and camera equal f . This $2f$ imaging system performs a spatial Fourier transform and maps the transverse momentum k^\perp into the transverse position r in the detector plane with the relation $r = \frac{f}{k} k^\perp$. Hence, the joint distribution $P(r_s, r_i)$ of observing a photon at position r_s with its partner at r_i is

$$P(r_s, r_i) \propto P_{\text{PDC}} \left(\frac{K}{f} r_s, \frac{K}{f} r_i \right), \quad (12)$$

where P_{PDC} is given in section 2. Similarly, the marginal distribution is given by

$$P(r_s) \propto \exp \left[-\frac{2\gamma L^2 K \Delta k}{f^2} \left(r_s - f \sqrt{\frac{\Delta k}{K}} \right)^2 \right], \quad (13)$$

and the same expression is applied to the idler marginal distribution. Equation (13) presents a ring with a diameter $f \sqrt{\Delta k / K}$ and width $f / (2L \sqrt{\gamma K \Delta k})$, as shown in the inset of figure 5. The conditional distribution is

$$P(r_s | r_i) \propto \exp \left(-\frac{w_0^2 K^2}{2f^2} |r_s + r_i|^2 \right), \quad (14)$$

the diameter (the full width at $1/e^2$ maximum) of the conditional distribution is

$$\Delta C \approx \frac{4f}{K w_0}. \quad (15)$$

In Type-I non-collinear PDC the photon pairs are emitted around cones centred on the beam propagation axis, z , and after the $2f$ system the cone is mapped to a circular section on the EMCCD, as shown in figures 4(a) and 5. Inside this section the photon pairs are anti-correlated with a correlation width ΔC .

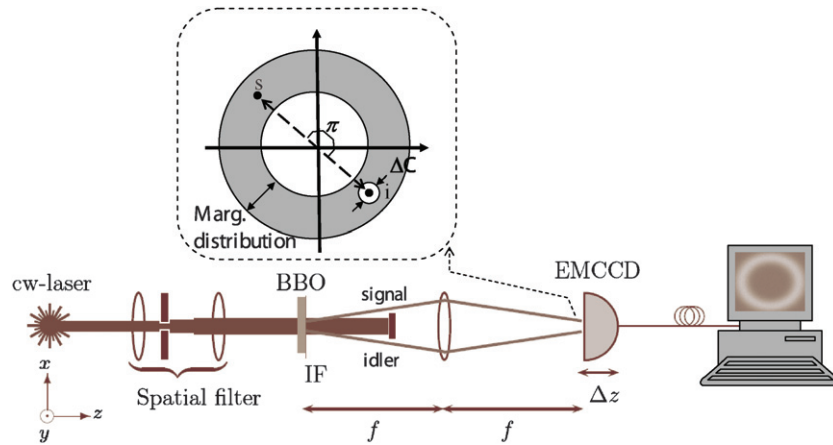


Figure 5. The experimental setup to study the spatial correlations of PDC with EMCCD. The downconverted photons propagate through a $2f$ imaging system and are detected by the EMCCD camera. The inset shows the distribution of the photons at the detection plane.

The EMCCD is configured for its best noise performance, with a vertical shift speed of $0.4 \mu\text{s}$, readout speed of 1 MHz and a temperature of $-75 \text{ }^\circ\text{C}$. The EM gain is set at the maximum level (~ 250). As mentioned in section 4.3, under these conditions the CIC is around 0.005 electrons/pixel/frame, which means there is one fake photon detection every 200 pixels. Although every quantum-optical application will have different requirements we can use this pixel number as an effective limit on the single-photon-detector array size and, thus as a benchmark to compare competing detector arrays. In our momentum correlation measurement we can avoid this limit by using a method introduced in [24], which employs the full area of the CCD. In this method the pump intensity is adjusted to allow several photon pairs reach the camera within one exposure time. The detected photon level is much less than 1 photon/pixel/frame to avoid two photons registering as one, while still bigger than the average CIC contribution in order to maintain a good signal-to-noise ratio. In the experiment, the detected photon level is chosen to be around 0.1 photon/pixel/frame. We operate the EMCCD in the photon counting mode, applying the thresholding technique to each frame. To characterize the transverse momentum correlations each thresholded frame $F(x, y)$ is convolved with itself in order to measure the overlap between this frame and its shifted mirror version $F(x_0 - x, y_0 - y)$. The individual frame convolutions are added together to give the total correlation

$$C_{\text{tot}}(x, y) = \sum_l^n F^l * F^l, \quad (16)$$

where $*$ denotes convolution and n is the number of frames. Since the photon pairs are anti-correlated in momentum, C_{tot} will exhibit a peak where the shift $(x_0, y_0) = (x_a, y_a)$ is such that each point in the ring in the original frame overlaps with the diametrically opposite point in the mirrored frame. After the accumulation of several frames, the contributions from noise are reduced, as it is completely uncorrelated, and one expects a peak with width ΔC will appear.

As an example, figure 6 shows the numerical simulation results for the total correlation C_{tot} . Each pixel of the EMCCD

is assumed to be an independent detector with the same performance. The pump beam waist is 2 mm which gives a correlation width $\Delta C = 7.8 \mu\text{m}$, i.e., a correlation area of one pixel. The graph in figure 6(a) is the correlation of just one frame, which is very noisy and it is not possible to retrieve any information about the momentum correlations. The general shape of the distribution arises from the convolution of two rings and is mainly due to photons whose twin has been lost. However, after the accumulation of 100 and 1000 frames (figures 6(b) and (c)), a distinct peak with width ΔC can be discerned at the centre of C_{tot} , which is the signature of the spatial correlation of PDC. We should indicate that since only the entangled photon pairs could contribute to the peak, it is not crucial for the input photon level to be greater than CIC. Still, a higher signal-to-noise ratio increases the height of the peak above the smooth background distribution.

5.2. Experiment results analysis

According to the numerical simulations, for the fixed input light level, the height of the correlation peak decreases rapidly with the increase of correlation width ΔC [24]. When ΔC is greater than 6 pixels, the peak is almost negligible. Since ΔC is inversely proportional to the pump beam width w_0 , it is advantageous to make the pump width as large as possible, while ensuring it still completely passes through the crystal aperture. To achieve this, w_0 is adjusted to be 0.5 mm, which gives a correlation width of around 2 pixels.

Figure 7 shows the experiment results for different input light levels and comparable simulation results. The simulation is run with the parameters of the experiment setup (noise level, gain, etc). The largest difference between the simulation and experiment is in the background levels, which is mostly due to noise. We believe this is due to small differences in the noise levels in the simulation and experiment. Although these are tiny, after a sum over 512×512 pixels, the difference becomes significant. Despite this difference, we expect that the smooth broad peak, due to the convolution of the ring structure, and the momentum correlation peak should be of equal size in simulation and experiment, as

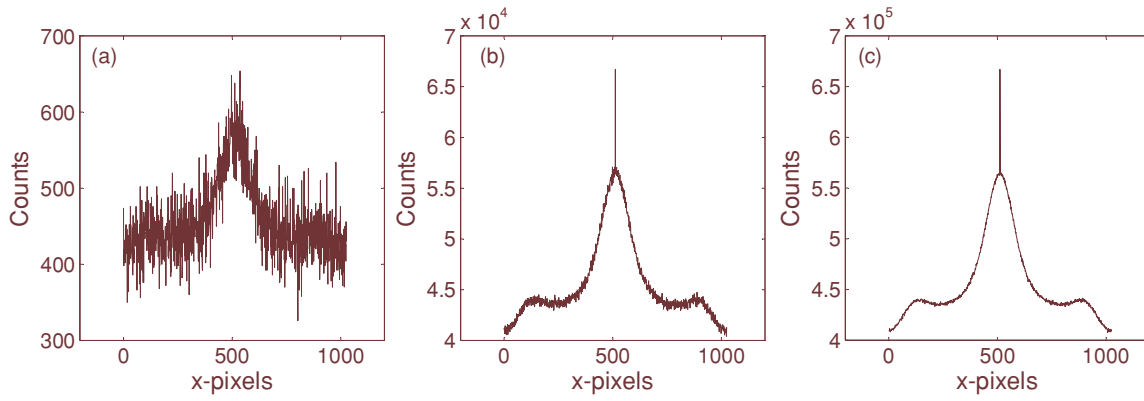


Figure 6. The 1D version of total correlation given by $C_{tot}(x_0, y_0)$ in equation (16). The number of frames analysed is (a) $n = 1$, (b) $n = 100$ and (c) $n = 1000$. The pump beam waist in this example was $w_0 = 2$ mm.

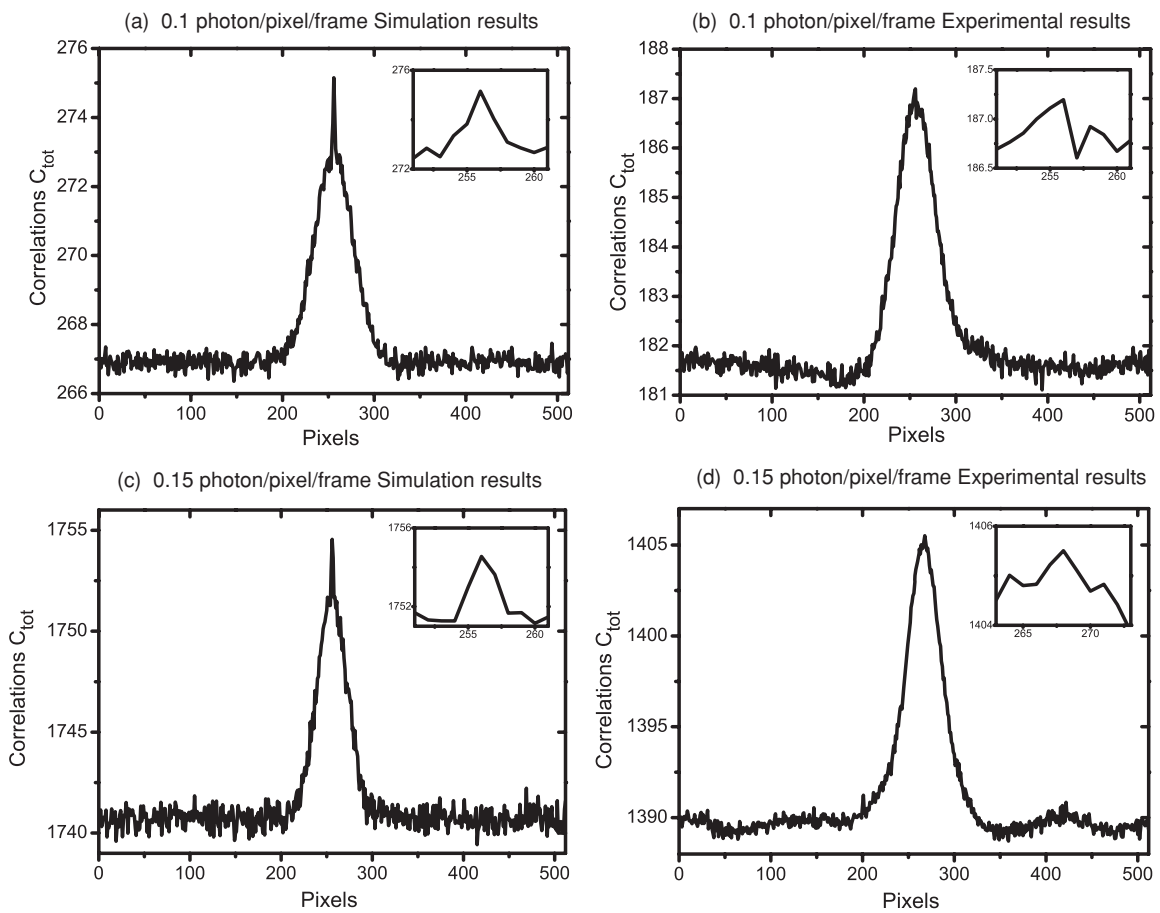


Figure 7. 1D correlations curves $C_{tot}(x_0, y_0)$ for the PDC set to two different levels of detected photons. (a) and (c) are the simulation results, while (b) and (d) are the experiment results. The insets in the figures are zoomed plots of the correlation peak.

they are. Although the simulation results indicate that there should be strong correlation peaks under these conditions, the experiment results are not as convincing. They do not show clear signatures of the correlation peaks that can be distinguished from noise fluctuations.

This could be due to a problem with EMCCDs that has recently been reported in connection with astronomical imaging. We call this the charge transfer efficiency (CTE) problem of EMCCD. For the previous simulations we assumed

that each pixel of EMCCD is an independent detector. This is not a completely accurate description of the situation. As shown in figure 1, the signal detected by every pixel will be transferred through the same shift register and gain register. The measure of the ability of the CCD to transfer the charge from one potential well to another is the CTE, and is typically less than 100%. If the charges do not move to the adjacent stages when they are supposed to, they will be left behind in one or more transfers and registered as if they are from

a different pixel. Although the CTE of each transfer could be high (over 0.9999) for large charge packets, after over a 1000 transfers, this will cause the noticeable spread of the charge from one pixel into adjacent pixels (for 0.9999 CTE, the spread will be over 2 pixels), introducing the crosstalk between different pixels, blurring the final image. Moreover, the CTE is usually worse at low signal levels. It has been reported that at below the 0.5 photon/pixel/frame input level, the CTE of a typical EMCCD could cause a spread of several pixels [15]. There is no doubt that this effect will increase the effective correlation width ΔC and, thus decrease the height of the correlation peak. Comparing the simulation results with the experiment results, we estimate the CTE induced spread is 2–3 pixels. This then defines the effective resolution of EMCCD for single-photon detection.

6. Conclusion

We experimentally tested the performance of the Andor iXon DV887 EMCCD camera for the detection of single-photon level input with the photon pairs generated from PDC. The camera exhibited single-photon sensitivity, good quantum efficiency and relatively low noise. Although we believe this electron multiplying camera's gain has been reduced by aging, it is still sufficient to allow the camera to work in the photon counting mode. In principle, the camera has a high resolution (512×512 pixels). However, it is possible that imperfect charge transfer efficiency broadens the effective pixels size and reduces the resolution by a factor of 2 or 3. The experiment results characterizing the spatial correlations of PDC provide evidence in support of this. With an improved CTE, EMCCD should be a good candidate for a single-photon-detector array. We should indicate that the camera used in our experiment is not a currently available model, but the methods can be applied to any EMCCD camera.

Acknowledgments

This work was supported by the EPSRC QIP-IRC, the EPSRC grant EP/C013840/1, and the EU integrated project QAP. LZ acknowledges the support from K C Wong scholarship. LN acknowledges the support from the Brazilian agency CNPq. IAW acknowledges the support from the Royal Society.

References

- [1] Zhang L, Silberhorn Ch and Walmsley I A 2008 *Phys. Rev. Lett.* **100** 110504
- [2] Ali-Khan I, Broadbent C J and Howell J C 2007 *Phys. Rev. Lett.* **98** 060503
- [3] Walborn S P, Lemelle D S, Almeida M P and Ribeiro P H S 2006 *Phys. Rev. Lett.* **96** 090501
- [4] Cerf N J, Bourennane M, Karlsson A and Gisin N 2002 *Phys. Rev. Lett.* **88** 127902
- [5] Yarnall T, Abouraddy A F, Saleh B E A and Teich M C 2007 *Phys. Rev. Lett.* **99** 170408
- [6] Cabello A 2006 *Phys. Rev. Lett.* **97** 140406
- [7] Zhang L *et al* 2007 *J. Mod. Opt.* **54** 707
- [8] Neves L, Lima G, Gómez J G Aguirre, Monken C H, Saavedra C and Pádua S 2005 *Phys. Rev. Lett.* **94** 100501
- [9] O'Sullivan-Hale M N, Khan I Ali, Boyd R W and Howell J C 2005 *Phys. Rev. Lett.* **94** 220501
- [10] Almeida M P, Walborn S P and Ribeiro P H Souto 2005 *Phys. Rev. A* **72** 022313
- [11] Monken C H, Ribeiro P H Souto and Pádua S 1998 *Phys. Rev. A* **57** 3123
- [12] Jiang L A, Dauler E A and Chang J T 2007 *Phys. Rev. A* **75** 062325
- [13] Jost B M, Sergienko A V, Abouraddy A F, Saleh B and Teich M 1998 *Opt. Express* **3** 81
- [14] Oemrawsingh S S R, van Druenen W J, Eliel E R and Woerdman J P 2002 *J. Opt. Soc. Am. B* **19** 2391
- [15] Tubbs R N 2003 Lucky exposures: diffraction limited astronomical imaging through the atmosphere *PhD Thesis* Cambridge University
- [16] Robbins M S and Hadwen B J 2003 *IEEE Trans. Electron Devices* **50** 1227
- [17] de Vree G A, Westra A H, Moody I, van der Have F, Ligtoet K M and Beekman F J 2005 *IEEE Trans. Nucl. Sci.* **52** 580
- [18] Basden A G, Haniff C A and Mackay C D 2003 *Mon. Not. R. Astron. Soc.* **345** 985
- [19] Teich M C, Matsuo K and Saleh B E A 1986 *IEEE J. Quantum Electron.* **QE-22** 1184
- [20] Janesick J R 2001 *Scientific Charge-Coupled Devices* (Bellingham, WA: SPIE)
- [21] E2V Technologies *Low Light Technical Note 4, Dark Signal and Clock-Induced Charge in L3Vision CCD Sensors* (<http://www.e2v.com/download.cfm?type=document&document=587>)
- [22] Tulloch S M 2004 *Proc. SPIE* **5492** 604
- [23] E2V Technologies *Low Light Technical Note 5, An Overview of the Ageing Characteristics of L3Vision Sensors* (<http://www.e2v.com/download.cfm?type=document&document=588>)
- [24] Neves L, Zhang L, Lundeen J S and Walmsley I A 2009, at press